Original

# Updating the Planar Patterson-Parker Table for Ir-192 and Cs-137 Brachytherapy Sources Using the Most Recent TG-43U1 Recommended Dosimetric Parameters

Naghshnezhad Z.[1]*, Faghihi R.[1], Mosleh-Shirazi M. A.[2], Meigooni A. S.[1,3]

[1]Department of Medical Radiation Engineering, Shiraz University, Shiraz, Iran
[2]Center for Research in Medical Physics and Biomedical Engineering, and Department of Radiotherapy, Shiraz University of Medical Sciences, Shiraz, Iran
[3]Comprehensive Cancer Center of Nevada, 3730 S. Eastern Dr., Las Vegas, NV, USA

## Abstract

**Background:** The Patterson-Parker table was created in 1934 to determine mg-hr required to deliver the prescribed dose to the treatment area. These tables were created using the dosimetric data for $^{226}$Ra that was determined in air and were utilized for dose calculations around implants with Ra-equivalent radionuclides such as $^{137}$Cs and $^{192}$Ir. Therefore, the differences of the tissue attenuation and anisotropy of these radionuclides and their impact on dose uniformity of the implants were ignored.

**Objective:** In this study, the Patterson-Parker table has been updated for $^{137}$Cs and $^{192}$Ir sources using their recent dosimetric data. Furthermore, the dose uniformity for different loading schemes, as a function of the implant area, was tested.

**Methods:** The updated Paterson-Parker tables were generated for $^{137}$Cs and $^{192}$Ir sources using their published dosimetric parameters that have been determined following the American Association of Physicists in Medicine (AAPM) Task group 43 (TG-43U1) recommendations. The accuracies of the updated tables were examined by two independent methods, Monte Carlo simulation technique and a commercially available treatment planning system. In addition to the dose values along the central axis of the implant, dose profiles along two orthogonal directions were evaluated for the selection of the optimal radioactivity distribution in an implant.

**Results:** We found that the original Paterson-Parker loading scheme of the radioactivity as a function of the implant size has to be adjusted to achieve the optimal dose distribution (1000 cGy ±10%) in an implant. In addition, it was shown that the same implant size for the mg-hr required for $^{137}$Cs was not identical to that of $^{192}$Ir. Similarly, there were some differences between the updated table and the published Paterson-Parkers tables. Independent Monte Carlo simulations and treatment planning data had excellent agreement with the updated data.

**Conclusion:** The conventional version of Paterson-Parker tables are not useful for the two commonly used brachytherapy sources. The updated version of the tables should be used instead.

## Keywords

Paterson-Parker table, TG-43, Dosimetry, Ir-192, Cs-137

## Introduction

Brachytherapy is one of the common radiation therapy techniques for malignant tumors. In this technique, the required radiation dose for the target area is delivered by placing the sources within the tumor or adjacent to it. Prior to the modern computerized treatment planning systems, brachytherapy was based on lookup tables. In 1934,

*Corresponding author: Zeinab Naghshnezhad, MSc, Department of Medical Radiation Engineering, School of Mechanical Engineering, Tel: +98-711-647-3474 Fax: +98-711-647-3474 E-mail: znaghsh@gmail.com

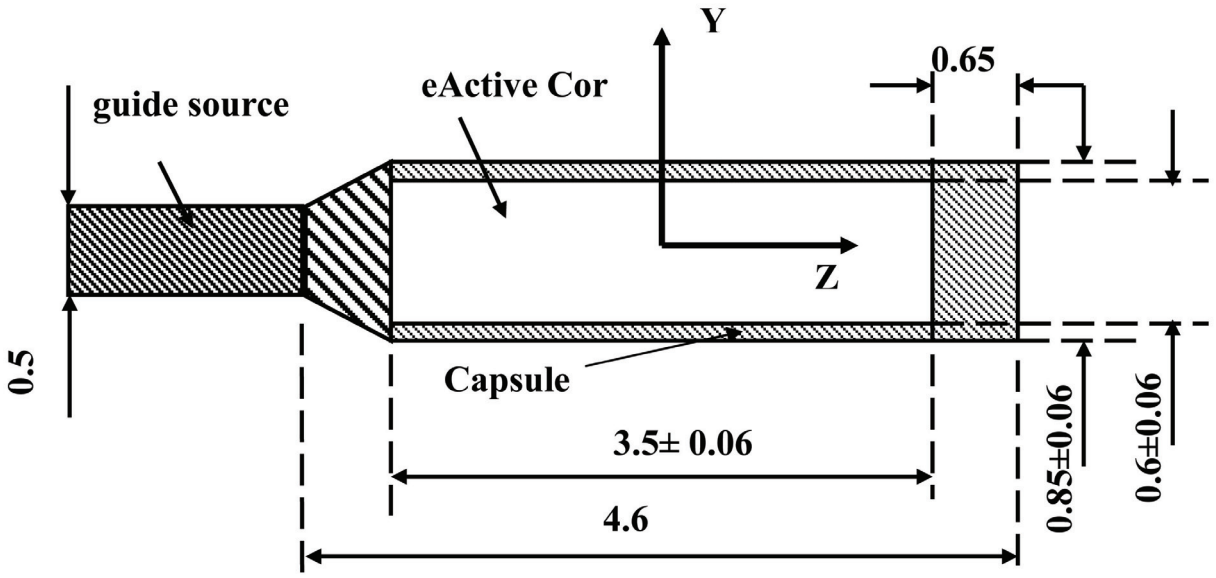


**Figure 1:** Schematic diagram of the high dose rate Flexisource $^{192}$Ir source (distances are given in mm)

Ralston Paterson and Herbert M. Parker created a table, then named after them Paterson-Parker or P-P table for determination of mg-hr that was needed to deliver a dose of 1000 R to the treatment area [1-3]. These tables were based on dosimetric data for $^{226}$Ra sources determined in air. The prescribed treatment area in this table was assumed to be at a distance h from the surface of the applicator. This table could presumably provide the dose uniformity within ±10% in the treatment area. Later on, this table was corrected by several investigators, first by utilizing dose rate constants of 8.4 R cm$^2$/mg-hr, for $^{226}$Ra in the original table, instead of 8.25 R cm$^2$/mg-hr. Thereafter, in the original table the conversion of exposure to dose was assumed to be unity and hence 1 cGy was assumed to be equal to 1 R. This was corrected by including exposure-to-dose conversion factors in order to achieve 1000 cGy rather than 1000 R [4].

The field of brachytherapy was later advanced by introduction of other sources such as $^{137}$Cs and $^{192}$Ir as alternatives to $^{226}$Ra. In addition, within the past decade, the protocols and algorithms of brachytherapy sources have been globally improved. The Task Group 43 of the American Association of Physicists in Medicine (AAPM) has published its original and updated reports (TG-43 [5], and TG-43U1 [6]) for low-energy brachytherapy sources in 1995, and 2004, respectively. Interestingly, several investigators have examined the feasibility of utilizing these recommendations for dosimetric evaluation of high-energy brachytherapy sources such as $^{137}$Cs and $^{192}$Ir [7-11]. Therefore, it is desirable to verify the accuracy of the Paterson-Parker tables for these sources with their most recently published dosimetric parameters.

In this study, the published TG-43U1 dosimetric parameters for two commercially available $^{137}$Cs and $^{192}$Ir sources were used to update the Paterson-Parker planner table. In order to verify the area of the coverage for each isotope, doses were calculated at several points away from the central axis of the plan, but located at the same height relative to the plane of implant. Moreover, in addition to the Paterson-Parker's recommendation for the distribution of the activity, the impact of some other activity distributions for optimal coverage of the treatment area was examined. The accuracy of the updated table was examined by two

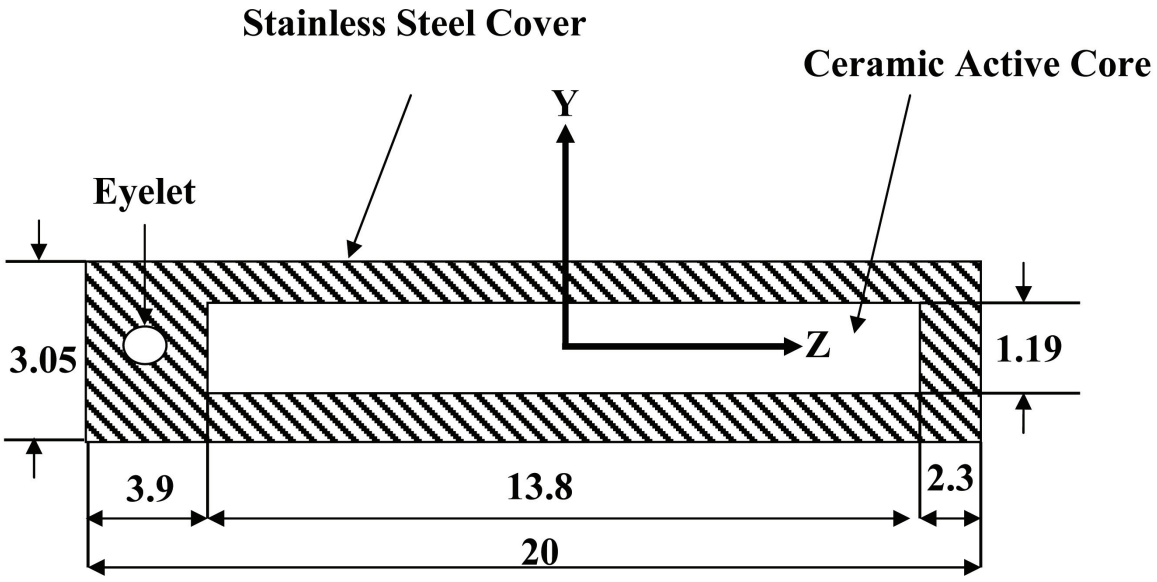


**Figure 2:** Schematic diagram of the low dose rate 3M $^{137}$Cs (model 6500/6D6C) source (dimensions are given in mm)

independent methods, Monte Carlo simulation technique and a commercially available treatment planning system.

## Materials and Methods

### Source Characteristics

In this work, the planar Patterson-Parker tables [1-3] were updated using the published TG-43U1 dosimetric parameters for high dose rate Flexisource $^{192}$Ir [9] (used in the Flexitron afterloading system, Isodose Control, Veenendaal, the Netherlands) and low dose rate Minnesota Mining and Manufacturing (3M) $^{137}$Cs (model 6500/6D6C, St. Paul, Minnesota, USA) [7] sources. The schematic diagram of the geometric design of the Flexisource $^{192}$Ir and 3M $^{137}$Cs sources are shown in Figures 1 and 2. According to the updated recommendations of TG-43 from AAPM (TG-43U1) [6], the source dimensions include the tolerances in the manufacturing process. For the Flexisource $^{192}$Ir source, the active core is made of a pure iridium cylinder (density 22.42 g/cm$^3$) with an active length of 3.5 mm and a diameter of 0.6 mm. The active core is covered by a stainless steel 304 capsule (composition by weight: Fe 67.92%, Cr 19%, Ni 10%, Mn 2%, Si 1% and C 0.08%, density 8 g/cm$^3$). Granero, *et al* [9], used a 5 mm in length and 0.5 mm in diameter cylinder stainless steel 304 cable for their Monte Carlo simulations. A similar source geometry was used in this study. For 3M $^{137}$Cs sources, the active core is a Zirconium phosphate glass cylinder (density 2.22 g/cm$^3$) with an active ceramic length of 13.8 mm and a diameter of 1.19 mm [7]. The active ceramic was covered by an AISI 316 stainless steel capsule (composition by weight: Si 2%, Cr 20%, Mn 2%, Fe 67%, Ni 9%, density 8.02 g/cm$^3$), leading to outer dimensions of the source of 3.05 mm in diameter and 20 mm of total length. The eyelet presented by this source was neglected in the simulations. In both sources, the Monte Carlo simulations were performed with the origin of the coordinate system placed at the center of the physical length of the source.

## Methodology

In this study, the integrated doses were calculated to several points above a planar implant, containing a matrix of n×m sources (where n and m were integers 2–10) for either

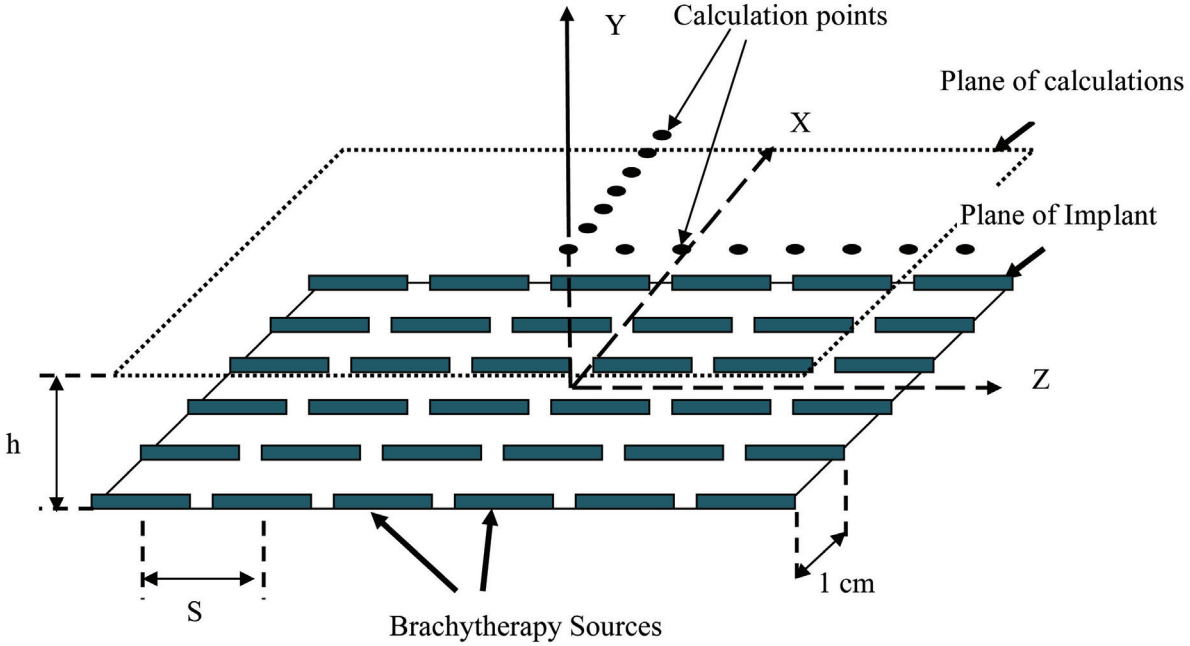


**Figure 3:** Schematic diagram of the brachytherapy source arrangements used for updating the Paterson-Parker planar table. In these arrangements the spacing between the source(s) was chosen to be 1 and 2 cm for $^{192}$Ir and $^{137}$Cs sources, respectively. Doses are calculated at distance h from the plane of implant.

$^{192}$Ir or $^{137}$Cs, using their most recent published TG-43U1 parameters [7, 9]. Figure 3 shows a schematic diagram of the source arrangements and the calculation points used in this study. The spacing between the sources on each row was selected to be 1 cm for $^{192}$Ir and 2 cm for $^{137}$Cs source (Fig. 3). The larger spacing for $^{137}$Cs was chosen to avoid the overlap of the sources. However, the spacing between the rows, for both source types, was chosen to be 1 cm. A comparison of dose profiles along the two orthogonal directions, X and Z axes, for several different distributions of the source strengths in the peripheral and middle of the implants, were used to achieve the maximum dose coverage from a given implant. The results of these distributions were compared with the values obtained using Patterson-Parker's recommendations [4] (Table 1).

**Table 1:** Paterson and Parker recommendation on the distribution of activity for a planar implant (Ref. 4)

| Area (cm²) | Fraction used in periphery |
|---|---|
| <25 | 2/3 |
| 25–100 | 1/2 |
| >100 | 1/3 |

For these calculations, the TG-43U1 formalism and dosimetric characteristics of each source model were incorporated in an MS Excel® spreadsheet. The orientations of the coordinate systems in these implants were selected in a way that they could easily match with the coordinate system used in TG-43U1 recommendation (*i.e.*, Z-axis is along the longitudinal direction of the source, and X and Y axes in the transverse directions) (Fig. 3). In addition, the origin of these coordinate systems was placed between the rows, approximately at the middle of the implant area.

For a planner implant, Manchester, Paterson and Parker defined the area of implant as the width of the implant times the active length, assuming that there were crossing needles on both ends of the implant [4, 22]. This area was then reduced by 10% for each uncrossed end. However, there was no clear transition

of the length and width of an implant when small seeds were used in place of a continuous active source. In our study, the active length (AL) and active width (AW) of the implant, following the TG-43U1 guidelines, were defined as:

$AL=n\times S1$

$AW=(m-1)\times S2$

where n represents the number of sources in each row and m is the number of rows in the implant; *S1* is center-to-center spacing between the sources in each row and *S2* is the spacing between the rows in the implant.

## Treatment Planning Procedures

To verify the accuracy of the updated Paterson-Parker table described previously, the integrated dose for two samples of implants with effective area of 20 and 90 $cm^2$ for $^{192}Ir$, and 180 $cm^2$ for $^{137}Cs$ sources was calculated using a commercially available treatment planning system. These calculations were performed by using the Eclipse, ver 8.1, treatment planning system (Varian Medical System Inc., Worldwide Headquarters, 3100 Hansen Way, Palo Alto, CA94304, USA). In these calculations the published TG-43U1 dosimetric parameters of the sources [7, 9] were first entered into the treatment planning system. The sources were then positioned in a planar arrangement with their locations and orientations identical to those mentioned above. In addition, the activity of each source, time period, and the calculation points were selected to be identical to the ones described in the Methodology section. The final doses derived from these calculations were compared with the values from the Methodology section and also Monte Carlo simulation as described below.

## Monte Carlo Simulations

Monte Carlo simulation is one of the most commonly used techniques for dosimetry of brachytherapy sources and implants. In this study, the MCNP Monte Carlo code (MCNP4C) was used to determine the integrated doses from two planar implants with 5×5 matrix (20 $cm^2$) of $^{192}Ir$ Flexisource and 4×8 matrix (56 $cm^2$) of $^{137}Cs$. The arrangements of the sources in these simulations were identical to those described in the Methodology section. The details of the Monte Carlo simulation technique are described below.

To establish the integrally of our Monte Carlo simulation technique, a single source simulation was performed with $^{192}Ir$ Flexisource and $^{137}Cs$. Their simulated TG-43U1 dosimetric parameters were compared with the published data. In these simulations, the source was placed at the center of a spherical water phantom with a radius of 40 cm, which acted as an unbounded phantom up to 20 cm of radial distance. The density of the water used in the simulation was 0.998 $g/cm^3$ at 22 °C, as is recommended in the TG-43U1. The $^{192}Ir$ gamma spectrum used in this study was obtained from the NuDat database [12]. In these simulations, it was assumed that the activities of the sources were uniformly distributed within the source core of the source. The beta spectrum of the $^{192}Ir$ source was not considered since its contribution to the dose rate distribution for distances greater than 1 mm from the source is negligible due to the encapsulation and the plastic catheter in which the source is introduced [13]. Collision KERMA was scored instead of the absorbed dose because in points where electronic equilibrium is achieved collision KERMA coincides with the absorbed dose. The cutoff energy used in the calculations was 10 keV for photons.

Simulations of the multi-source planar implants were performed after demonstrating the success of single source dosimetry for $^{192}Ir$ and $^{137}Cs$ sources. Since, MCNP does not allow variable source activity within one implant, these simulations were performed using two separate sections—one with peripheral sources and another with central sources. The total integrated dose for each point was calculated as a summation of dose contributions

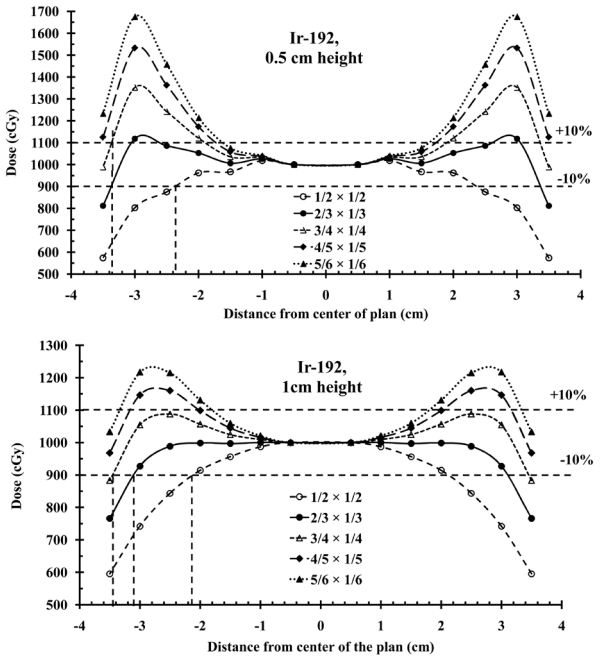


**Figure 4:** Comparison of dose profiles along the Z-axis at 0.5 and 1 cm away from a 7×7 $^{192}$Ir planar implant (42 cm$^2$) with different distribution of source strength on the periphery and inside the implant.

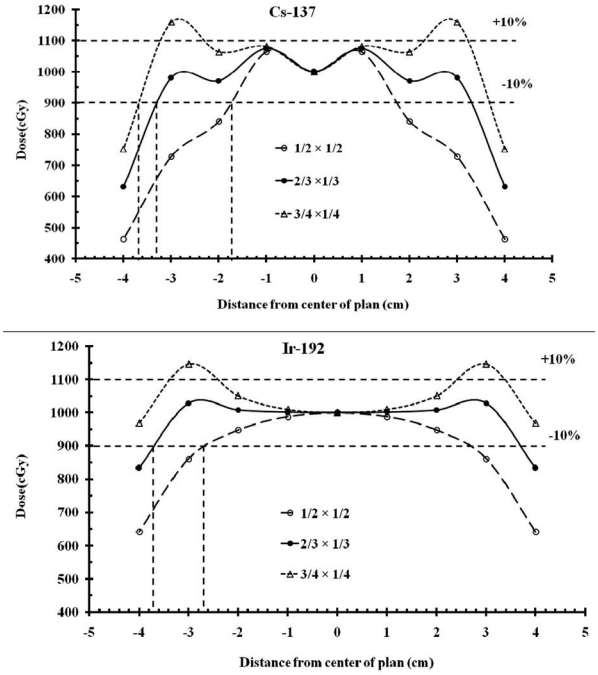


**Figure 5:** Comparison of dose profiles along the X-axis at 1 cm away from a 56 cm$^2$ $^{137}$Cs (the upper panel) and $^{192}$Ir (the lower panel) planar implants as a function of different loading scheme for the peripheral and central aspect of the implant.

from each simulation. These simulations were performed using "*f4" Tally with the mass absorption coefficient taken from tabulated data by Hubble and Seltzer [14]. A "conversion factor" was calculated for each source model, following the guidelines of Zhang, *et al* [15], in order to take the mg-hr of each source into account as well as the self absorption of the source. In addition, the correction for the self absorption of each source type was calculated as a ratio of the simulated KERMA rate at a given point for a single source with its true geometric and chemical structure to the KERMA rate at the same point from an imaginary source with identical geometry but all the components were replaced by air. Care was taken to have the same amount of the radioactivity contained in both source geometries. The self absorption of $^{192}$Ir, and $^{137}$Cs sources were found to be 11% and 3.5%, respectively. With these corrections, the results of the Monte Carlo simulations for multi-source planar implants were corrected for the self absorption of single sources and they were not required to be normalized to in-air simulations.

## Results

Figure 4 shows a comparison of dose profiles, along the Z-axis at distances of 0.5 cm and 1.0 cm from a 7×7 $^{192}$Ir planner implant with different distributions of the source strengths in the peripheral and central part of the implant. These graphs also show the loading schemes that provided the dose profile with ±10% deviation from the central dose. Moreover, these results indicated that at 1 cm height, the length of the area (*i.e.*, twice the distance from the center) was covered by the prescribed dose (1000 cGy ±10% in this case) is 4.2, 6.2, and 7.0 cm for 1/2×1/2, 2/3×1/3, and 3/4×1/4 loading scheme, respectively. However, for a height of 0.5 cm, the coverage was 4.6 and 6.2 cm for 1/2×1/2 and 2/3×1/3 loading scheme, respectively, and the 3/4×1/4

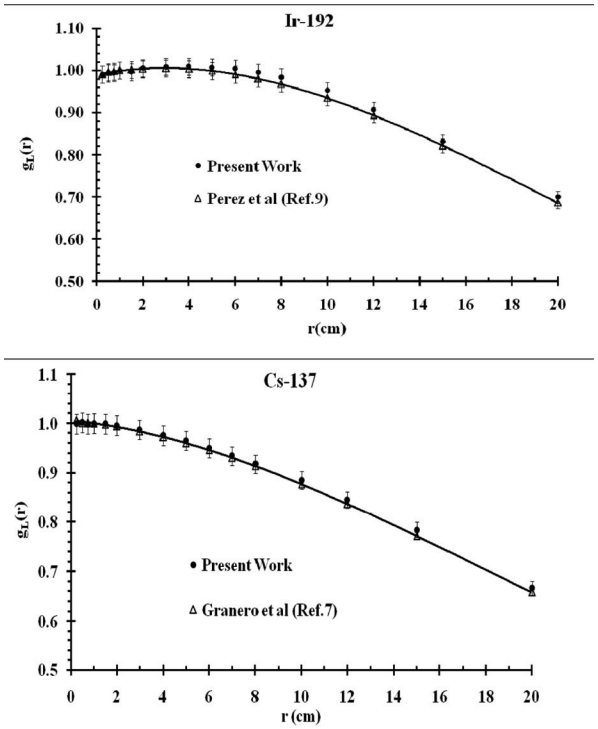


**Figure 6:** Comparison of Monte Carlo simulated radial dose functions of the high dose rate Flexisource $^{192}$Ir source (the upper panel) and $^{137}$Cs source (the lower panel) with data published by Granero, *et al* [9], and Perez, *et al* [7], respectively. The error bar in the graph is within 2% of uncertainty associated with the present data; the solid and dashed curves are 3rd degree polynomial fits through the data points just to guide the eye.

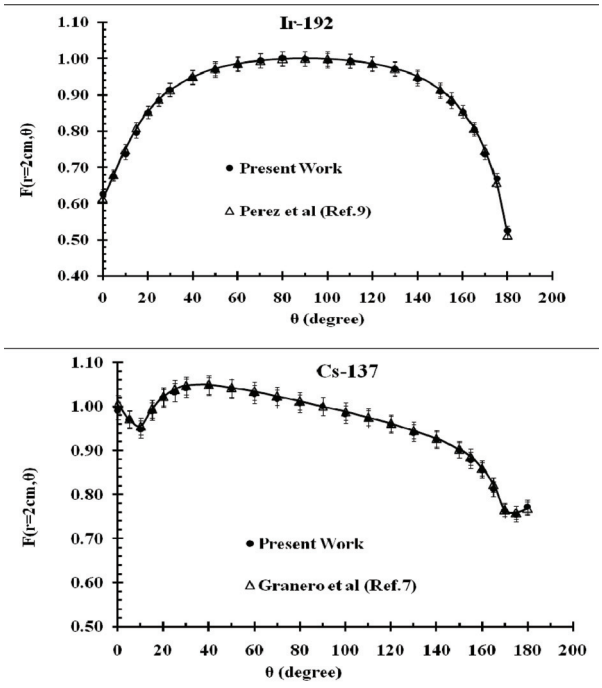


**Figure 7:** Comparison of Monte Carlo simulated 2D anisotropy functions of the high dose rate Flexisource $^{192}$Ir source (the upper panel) and $^{137}$Cs source (the lower panel) with data published by Granero, *et al* [9], and Perez, *et al* [7], respectively. The error bar in the graph is within 2% of uncertainty associated with the present data; the solid curve is a 4th degree polynomial fit to the present data, just to guide the eye.

loading scheme was not appropriate.

In this study, we also determined the dose profiles of both $^{137}$Cs and $^{192}$Ir for the same implant area and different distributions of the source strengths. Figure 5 shows a sample of these comparisons for a 56-cm$^2$ implant area. These results indicated that for both source types, the loading scheme of the 2/3×1/3 for the peripheral and central source strength provided a better coverage than the 1/2×1/2 suggested by Paterson and Parker.

Monte Carlo simulations were validated by simulating single source TG-43U1 parameters for both $^{137}$Cs and $^{192}$Ir sources. Table 2 shows the comparison of dose rate constants of these sources with the published data [7, 9]. In addi-

**Table 2:** Comparison of Monte Carlo simulated dose rate constant determined in this study for 3M $^{137}$Cs and Flexisource $^{192}$Ir sources with data published by Perez, *et al* [7], and Granero *et al* [9], respectively.

| Source | Dose rate constant (cGy h$^{-1}$ U$^{-1}$) | | | Difference (%) |
|---|---|---|---|---|
| | Present work (MCNP4c) | Ref 7 (GEANT4) | Ref 9 (GEANT4) | |
| $^{192}$Ir | 1.12 | – | 1.109 | 1.4 |
| $^{137}$Cs | 0.964 | 0.96 | – | 0.4 |

**Table 3:** Comparison of Monte Carlo simulated integrated dose on the central axis and several off-axis points for a 5×5 source (20 $cm^2$) $^{192}Ir$ implant, with the calculated data using an MS Excel® spreadsheet program using published TG-43U1 parameters [9]. These calculations were performed using a 2/3×1/3 source strength distribution.

| Position (cm) (X,Y,Z) | Excel (cGy) | Monte Carlo (cGy) | Difference (%) |
|---|---|---|---|
| (0,1,0) | 1000 | 1018 | -1.80 |
| (0,1,1) | 1000 | 1011 | -1.10 |
| (1,1,0) | 1000 | 1027 | -2.70 |
| (1,1,1) | 1000 | 985 | 1.50 |
| (0,1,2) | 907 | 915 | -0.88 |
| (2,1,0) | 908 | 916 | -0.88 |
| (2,1,2) | 822 | 824 | -0.24 |
| (0,1,3) | 633 | 643 | -1.58 |
| (3,1,0) | 645 | 649 | -0.62 |
| (1,1,3) | 633 | 641 | -1.26 |
| (2,1,3) | 571 | 586 | -2.63 |
| (3,1,3) | 417 | 427 | -2.40 |

tion, Figure 6 shows a good agreement (within ±2%) between the Monte Carlo simulated radial dose function of single $^{137}Cs$ and $^{192}Ir$ sources in obtained in this study and published data by Perez, *et al* [7], and Granero, *et al* [9], respectively. Figure 7 shows a good agreement (within ±2%) between the new Monte Carlo simulated 2D anisotropy function of these sources at a radial distance of 2 cm relative to the source center and the published data [7, 9]. There was also a good agreement between Monte Carlo simulated dosimetric data for each source model and published data that confirmed the accuracy of sources geometry and parameters used in the simulations. The validated Monte Carlo simulations were used for simulation of a multi-seed implant. Tables 3 and 4 compare the Monte Carlo simulated and TG-43U1-based calculated-dose profiles for a 5×5 $^{192}Ir$ planar implant and a 4×8 $^{137}Cs$ planar implant with effective areas of 20 and 56 $cm^2$, respectively, at height of 1 cm. The results reflected excellent agreement (within ±5%) between the two methods.

**Table 4:** Comparison of Monte Carlo simulated integrated dose on the central axis and several off-axis points for a 4×8 source (56 $cm^2$) $^{137}Cs$ implant, with the calculated data using an MS Excel® spreadsheet program using published TG-43U1 parameters [7]. These calculations were performed using a 2/3×1/3 source strength distribution.

| Position (cm) (X,Y,Z) | Excel (cGy) | Monte Carlo (cGy) | Difference (%) |
|---|---|---|---|
| (0,1,0) | 1000 | 984 | 1.60 |
| (0,1,1) | 961 | 974 | -1.35 |
| (0,1,-1) | 961 | 954 | 0.73 |
| (1,1,0) | 1074 | 1045 | 2.70 |
| (-1,1,0) | 1074 | 1035 | 3.63 |
| (0,1,2) | 936 | 919 | 1.82 |
| (0,1,-2) | 936 | 926 | 1.07 |
| (1,1,2) | 1011 | 975 | 3.56 |
| (1,1,-2) | 1011 | 990 | 2.08 |
| (2,1,0) | 971 | 959 | 1.24 |
| (-2,1,0) | 971 | 938 | 3.40 |
| (2,1,2) | 907 | 904 | 0.33 |
| (2,1,-2) | 907 | 897 | 1.10 |
| (0,1,3) | 824 | 815 | 1.09 |
| (0,1,-3) | 824 | 825 | -0.12 |
| (3,1,0) | 979 | 935 | 4.49 |
| (-3,1,0) | 979 | 947 | 3.27 |
| (3,1,2) | 921 | 916 | 0.54 |
| (3,1,-2) | 921 | 879 | 4.56 |
| (0,1,4) | 615 | 594 | 3.41 |
| (0,1,-4) | 615 | 582 | 5.37 |
| (4,1,0) | 632 | 614 | 2.85 |
| (-4,1,0) | 632 | 641 | -1.42 |
| (4,1,2) | 587 | 570 | 2.90 |
| (4,1,-2) | 587 | 581 | 1.02 |

The accuracy of the values calculated with TG-43U1 parameters in an MS Excel® spreadsheet was also confirmed by comparing the dose profiles for two samples of a planar implant with the values obtained using a commercially available system. Tables 5 and 6 show good agreement (within ±2%) between the two methods for a 10×10 and 5×5 planar implants of $^{192}Ir$ sources. Similar level of agreement (within ±3%) was observed for $^{137}Cs$ sources (Table 7).

Once the methodology of our calculations

**Table 5:** Comparison of the integrated dose on the central axis and several off-axis points of a 10×10 (90 $cm^2$) $^{192}Ir$ planner implant, calculated using published TG-43U1 parameters [9] by an MS Excel® spreadsheet program and a commercially available treatment planning system. These calculations were performed using a 1/2×1/2 source strength distribution.

| Position (cm) (X,Y,Z) | TG-43U1 (cGy) | Treatment planning (cGy) | Difference (%) |
|---|---|---|---|
| (0,1,0) | 1000 | 982 | 1.80 |
| (1,1,0) | 995 | 977 | 1.81 |
| (0,1,1) | 995 | 978 | 1.71 |
| (1,1,1) | 990 | 973 | 1.72 |
| (2,1,0) | 979 | 962 | 1.74 |
| (0,1,2) | 981 | 964 | 1.73 |
| (3,1,0) | 954 | 937 | 1.78 |
| (0,1,3) | 959 | 942 | 1.77 |
| (0,1,4) | 920 | 902 | 1.96 |
| (0,1,5) | 712 | 698 | 1.97 |
| (4,1,0) | 910 | 894 | 1.76 |
| (3,1,3) | 909 | 893 | 1.76 |
| (4,1,4) | 799 | 784 | 1.88 |
| (1,1,5) | 707 | 694 | 1.84 |
| (2,1,5) | 692 | 678 | 2.02 |
| (3,1,5) | 659 | 647 | 1.82 |
| (4,1,5) | 592 | 580 | 2.03 |

was tested by Monte Carlo simulation and also a commercially available treatment planning software, the calculations were performed for determination of mg-hrs of different implant sizes for each source type. Tables 8 and

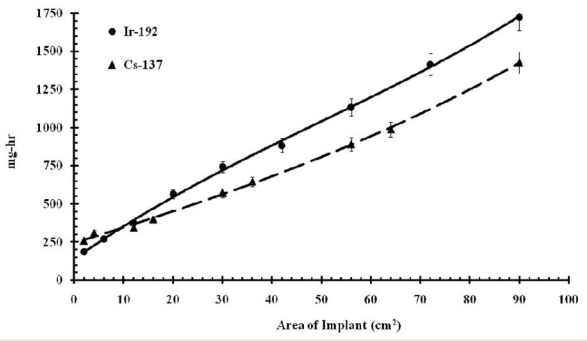


**Figure 8:** Comparison of mg-hrs for $^{192}Ir$ *vs* $^{137}Cs$ as a function of the implant area to deliver 1000 cGy at 1 cm away from a planar implant.

**Table 6:** Comparison of the integrated dose on the central axis and several off-axis points of a 5×5 source (20 $cm^2$) $^{192}Ir$ implant calculated using published TG-43U1 parameters [9] by an MS Excel® spreadsheet program and a commercially available treatment planning system. The calculations were performed using a 2/3×1/3 source strength distribution.

| Position (cm) (X,Y,Z) | TG-43U1 (cGy) | Treatment planning (cGy) | Difference (%) |
|---|---|---|---|
| (0,1,0) | 1000 | 995 | 0.50 |
| (1,1,0) | 1000 | 995 | 0.50 |
| (0,1,1) | 1000 | 995 | 0.50 |
| (1,1,1) | 1000 | 995 | 0.50 |
| (2,1,0) | 908 | 903 | 0.55 |
| (0,1,2) | 907 | 902 | 0.55 |
| (2,1,2) | 822 | 817 | 0.61 |
| (3,1,0) | 645 | 641 | 0.62 |
| (0,1,3) | 633 | 630 | 0.47 |
| (1,1,3) | 633 | 630 | 0.47 |
| (2,1,3) | 571 | 568 | 0.53 |
| (3,1,3) | 417 | 415 | 0.48 |

9 show the updated Paterson-Parker tables for high dose rate Flexisource $^{192}Ir$ and low dose rate 3M $^{137}Cs$, respectively; the generated data was based on their most recent published TG-

**TABLE 7:** Comparison between treatment planning results and MS Excel® calculated dose for a 10×10 seed (180 $cm^2$) $^{137}Cs$ with a 1/2×1/2 source strength distribution.

| Position (cm) (X,Y,Z) | TG-43U1 (cGy) | Treatment planning (cGy) | Difference (%) |
|---|---|---|---|
| (0,1,0) | 1000 | 1022 | -2.20 |
| (1,1,0) | 995 | 1017 | -2.21 |
| (0,1,2) | 997 | 1020 | -2.31 |
| (1,1,2) | 992 | 1014 | -2.22 |
| (2,1,0) | 980 | 1001 | -2.14 |
| (0,1,4) | 990 | 1013 | -2.32 |
| (2,1,4) | 970 | 991 | -2.16 |
| (3,1,0) | 955 | 975 | -2.09 |
| (0,1,6) | 986 | 1007 | -2.13 |
| (3,1,6) | 936 | 955 | -2.03 |
| (4,1,0) | 913 | 928 | -1.64 |
| (0,1,8) | 1033 | 1050 | -1.65 |
| (4,1,8) | 884 | 899 | -1.70 |

**Table 8:** Updated Paterson-Parker table for high dose rate Flexisource $^{192}$Ir. The values represent the mg-hrs of the source required to deliver 1000 cGy to a given distance from the planar implant.

| Area ($cm^2$) | Distance from the planar implant (cm) | | | | | | | | |
|---|---|---|---|---|---|---|---|---|---|
| | 0 | 0.5 | 1 | 1.5 | 2 | 2.5 | 3 | 3.5 | 4 |
| 4 | 86 | 123 | 228 | 392 | 613 | 894 | 1234 | 1636 | 2101 |
| 5 | 97 | 138 | 249 | 418 | 642 | 925 | 1267 | 1670 | 2136 |
| 6 | 108 | 152 | 269 | 443 | 671 | 956 | 1300 | 1704 | 2171 |
| 7 | 122 | 168 | 287 | 462 | 690 | 975 | 1319 | 1724 | 2191 |
| 8 | 136 | 184 | 305 | 481 | 709 | 995 | 1339 | 1743 | 2210 |
| 9 | 150 | 200 | 323 | 500 | 729 | 1014 | 1358 | 1763 | 2230 |
| 10 | 164 | 215 | 341 | 518 | 748 | 1033 | 1377 | 1782 | 2249 |
| 12 | 192 | 247 | 377 | 556 | 786 | 1072 | 1416 | 1821 | 2288 |
| 14 | 227 | 287 | 424 | 609 | 844 | 1134 | 1481 | 1876 | 2359 |
| 16 | 263 | 327 | 471 | 662 | 902 | 1196 | 1547 | 1930 | 2429 |
| 18 | 298 | 366 | 517 | 714 | 959 | 1257 | 1612 | 1985 | 2500 |
| 20 | 333 | 406 | 564 | 767 | 1017 | 1319 | 1677 | 2039 | 2570 |
| 24 | 384 | 466 | 635 | 846 | 1100 | 1405 | 1765 | 2150 | 2661 |
| 28 | 435 | 525 | 706 | 925 | 1183 | 1491 | 1852 | 2261 | 2752 |
| 30 | 460 | 555 | 742 | 964 | 1225 | 1534 | 1896 | 2316 | 2797 |
| 34 | 489 | 590 | 789 | 1022 | 1293 | 1610 | 1979 | 2406 | 2893 |
| 38 | 519 | 626 | 836 | 1079 | 1360 | 1685 | 2062 | 2495 | 2988 |
| 40 | 533 | 643 | 860 | 1108 | 1394 | 1723 | 2104 | 2540 | 3036 |
| 44 | 574 | 691 | 919 | 1177 | 1471 | 1806 | 2192 | 2634 | 3135 |
| 48 | 627 | 751 | 990 | 1257 | 1557 | 1897 | 2287 | 2732 | 3236 |
| 50 | 654 | 782 | 1025 | 1296 | 1599 | 1943 | 2334 | 2780 | 3286 |
| 54 | 707 | 842 | 1096 | 1376 | 1685 | 2034 | 2429 | 2878 | 3387 |
| 58 | 759 | 902 | 1167 | 1456 | 1772 | 2126 | 2527 | 2981 | 3494 |
| 60 | 785 | 931 | 1202 | 1495 | 1816 | 2174 | 2577 | 3034 | 3550 |
| 64 | 837 | 990 | 1272 | 1575 | 1903 | 2269 | 2678 | 3141 | 3661 |
| 68 | 889 | 1049 | 1342 | 1654 | 1991 | 2363 | 2779 | 3248 | 3773 |
| 70 | 915 | 1079 | 1377 | 1693 | 2034 | 2411 | 2830 | 3302 | 3828 |
| 74 | 967 | 1137 | 1447 | 1772 | 2120 | 2503 | 2928 | 3405 | 3935 |
| 78 | 1019 | 1196 | 1516 | 1850 | 2205 | 2594 | 3023 | 3504 | 4037 |
| 80 | 1045 | 1225 | 1550 | 1889 | 2247 | 2639 | 3071 | 3554 | 4088 |
| 84 | 1097 | 1284 | 1619 | 1966 | 2332 | 2730 | 3167 | 3653 | 4191 |
| 88 | 1149 | 1343 | 1688 | 2044 | 2417 | 2821 | 3262 | 3752 | 4293 |
| 90 | 1175 | 1372 | 1723 | 2083 | 2459 | 2866 | 3310 | 3802 | 4344 |

43U1 dosimetric parameters. Like the original Paterson-Parker table, the values in these tables represent the mg-hrs for each source type that is required to deliver 1000 cGy to a given distance on the central axis of the planar implants. Figure 8 shows a comparison of the mg-hrs obtained in this technique for $^{192}$Ir and $^{137}$Cs sources, as a function of implant area.

Tables 11 and 12 compare the updated Paterson-Parker table for $^{192}$Ir and $^{137}$Cs with the original table. The results indicated that for $^{192}$Ir and $^{137}$Cs sources, there are approxi-

**Table 9:** Updated Paterson-Parker table for low dose rate 3M $^{137}$Cs. The values represent the mg-hrs of the source required to deliver 1000 cGy to a given distance from the planner implant.

| Area ($cm^2$) | Distance from the planar implant (cm) | | | | | | | | |
|---|---|---|---|---|---|---|---|---|---|
| | 0 | 0.5 | 1 | 1.5 | 2 | 2.5 | 3 | 3.5 | 4 |
| 4 | 139 | 187 | 310 | 489 | 726 | 1052 | 1389 | 1820 | 2320 |
| 5 | 142 | 191 | 315 | 494 | 731 | 1054 | 1394 | 1825 | 2326 |
| 6 | 146 | 195 | 319 | 499 | 736 | 1056 | 1400 | 1831 | 2331 |
| 7 | 149 | 199 | 324 | 503 | 741 | 1057 | 1405 | 1836 | 2337 |
| 8 | 153 | 203 | 328 | 508 | 746 | 1059 | 1410 | 1842 | 2342 |
| 9 | 156 | 206 | 333 | 513 | 751 | 1061 | 1415 | 1847 | 2348 |
| 10 | 159 | 210 | 337 | 518 | 756 | 1063 | 1421 | 1852 | 2353 |
| 12 | 166 | 218 | 346 | 527 | 766 | 1066 | 1431 | 1863 | 2364 |
| 14 | 183 | 238 | 373 | 561 | 806 | 1111 | 1480 | 1915 | 2420 |
| 16 | 199 | 258 | 399 | 594 | 845 | 1156 | 1529 | 1967 | 2475 |
| 18 | 215 | 277 | 424 | 624 | 880 | 1195 | 1571 | 2012 | 2523 |
| 20 | 230 | 295 | 448 | 654 | 914 | 1233 | 1614 | 2058 | 2571 |
| 24 | 261 | 333 | 497 | 714 | 984 | 1311 | 1698 | 2148 | 2666 |
| 28 | 292 | 370 | 546 | 774 | 1053 | 1388 | 1783 | 2239 | 2762 |
| 30 | 308 | 389 | 571 | 804 | 1088 | 1427 | 1825 | 2284 | 2810 |
| 34 | 341 | 428 | 620 | 865 | 1122 | 1506 | 1910 | 2376 | 2907 |
| 38 | 375 | 468 | 670 | 922 | 1174 | 1576 | 1985 | 2456 | 2991 |
| 40 | 393 | 488 | 694 | 950 | 1209 | 1607 | 2018 | 2489 | 3025 |
| 44 | 429 | 529 | 743 | 1004 | 1279 | 1669 | 2083 | 2556 | 3094 |
| 48 | 466 | 571 | 792 | 1059 | 1348 | 1732 | 2147 | 2623 | 3163 |
| 50 | 484 | 591 | 817 | 1086 | 1383 | 1763 | 2180 | 2657 | 3198 |
| 54 | 520 | 632 | 866 | 1141 | 1453 | 1825 | 2245 | 2724 | 3267 |
| 58 | 556 | 673 | 915 | 1197 | 1521 | 1892 | 2316 | 2799 | 3346 |
| 60 | 573 | 694 | 939 | 1226 | 1553 | 1928 | 2355 | 2841 | 3391 |
| 64 | 608 | 734 | 988 | 1283 | 1618 | 1999 | 2433 | 2925 | 3480 |
| 68 | 658 | 791 | 1055 | 1359 | 1703 | 2091 | 2532 | 3030 | 3590 |
| 70 | 682 | 819 | 1088 | 1398 | 1745 | 2137 | 2581 | 3082 | 3645 |
| 74 | 732 | 876 | 1155 | 1474 | 1829 | 2229 | 2679 | 3186 | 3755 |
| 78 | 781 | 932 | 1222 | 1550 | 1914 | 2321 | 2778 | 3291 | 3865 |
| 80 | 806 | 961 | 1256 | 1588 | 1956 | 2366 | 2827 | 3343 | 3920 |
| 84 | 856 | 1017 | 1323 | 1665 | 2040 | 2458 | 2925 | 3447 | 4030 |
| 88 | 905 | 1074 | 1390 | 1741 | 2125 | 2550 | 3024 | 3552 | 4140 |
| 90 | 930 | 1102 | 1423 | 1779 | 2167 | 2596 | 3073 | 3604 | 4195 |
| 120 | 971 | 1160 | 1515 | 1907 | 2330 | 2790 | 3296 | 3854 | 4468 |

mately 25% and 35% difference between the table values, respectively. These differences might be attributed to the updated source information, as well as the selection of a proper distribution of the source strengths for a better coverage of the implanted area.

## Discussion

The clinical application of brachytherapy is based on a limited unique methodology describing the distribution of source strength within an implanted area or volume to achieve

**Table 10:** The Optimal distribution of the source strength used in the updated Paterson-Parker table.

| Implant area ($cm^2$) | Peripheral loading | Central loading |
|---|---|---|
| <20 | 4/5 | 1/5 |
| 20–42 | 3/4 | 1/4 |
| 43–90 | 2/3 | 1/3 |

the desired dose delivery. Paterson-Parker system [1], Quimby System [16], and Paris system [17] are the most commonly used systems in conventional brachytherapy. The linear, planar, and volume tables of the Paterson-Parkers have been used widely round the globe for many years. It is interesting that these tables were created for determining the mg-hrs for all high energy brachytherapy sources, for which the Compton interaction was dominant. These tables did not differentiate between various radionuclides sources such as $^{137}Cs$ and $^{192}Ir$. Innovative radiation dosimetry expanded [5, 6] and technological advancements in equipment manufacturing permitted us to obtain very detailed distributions of radiation from variety of sources [19-21]. Old systems were replaced by computerized planning systems. However, many clinicians still use the traditional methods and old Paterson-Parker tables either as their primary method of planning or as a tool for the second check of a plan.

In this study, the Paterson-Parker planar table was updated using the most recent published TG-43U1 dosimetric parameters of the commercially available high dose rate Flexisource $^{192}Ir$ and low dose rate 3M $^{137}Cs$ brachytherapy sources. A schematic diagram explaining the pattern of distribution of the sources used in this study is shown in Figure 3. In addition to the integrated dose at the central axis of the planar implants, dose profiles in two orthogonal directions were calculated for different distributions of source strengths. The results

**Table 11:** Comparison of the new table for $^{192}Ir$ and P-P table [1]

| Area ($cm^2$) | Distance from the planar implant (cm) | | | | | | | | | | | |
|---|---|---|---|---|---|---|---|---|---|---|---|---|
| | 1 | | | 2 | | | 3 | | | 4 | | |
| | Updated | P-P | Dif% | Updated | P-P | Dif% | Updated | P-P | Dif% | Updated | P-P | Dif% |
| 1 | 156 | 182 | 14 | 524 | 571 | 8 | 1137 | 1204 | 6 | 2000 | 2100 | 5 |
| 2 | 187 | 227 | 18 | 555 | 632 | 12 | 1168 | 1274 | 8 | 2031 | 2172 | 6 |
| 3 | 208 | 263 | 21 | 584 | 689 | 15 | 1201 | 1331 | 10 | 2066 | 2241 | 8 |
| 4 | 228 | 296 | 23 | 613 | 743 | 17 | 1234 | 1388 | 11 | 2101 | 2307 | 9 |
| 5 | 249 | 326 | 24 | 642 | 787 | 18 | 1267 | 1436 | 12 | 2136 | 2369 | 10 |
| 6 | 269 | 354 | 24 | 671 | 832 | 19 | 1300 | 1495 | 13 | 2171 | 2432 | 11 |
| 7 | 287 | 382 | 25 | 690 | 870 | 21 | 1319 | 1547 | 15 | 2191 | 2490 | 12 |
| 8 | 305 | 409 | 25 | 709 | 910 | 22 | 1339 | 1596 | 16 | 2210 | 2548 | 13 |
| 9 | 323 | 434 | 26 | 729 | 946 | 23 | 1358 | 1645 | 17 | 2230 | 2605 | 14 |
| 10 | 341 | 461 | 26 | 748 | 982 | 24 | 1377 | 1692 | 19 | 2249 | 2660 | 15 |
| 20 | 564 | 682 | 17 | 1017 | 1303 | 22 | 1677 | 2106 | 20 | 2570 | 3155 | 19 |
| 30 | 742 | 846 | 12 | 1225 | 1582 | 23 | 1896 | 2468 | 23 | 2797 | 3562 | 21 |
| 40 | 860 | 994 | 13 | 1394 | 1843 | 24 | 2104 | 2787 | 25 | 3036 | 3931 | 23 |
| 50 | 1025 | 1141 | 10 | 1599 | 2083 | 23 | 2334 | 3082 | 24 | 3286 | 4275 | 23 |
| 60 | 1202 | 1283 | 6 | 1816 | 2319 | 22 | 2577 | 3362 | 23 | 3550 | 4605 | 23 |
| 70 | 1377 | 1426 | 3 | 2034 | 2532 | 20 | 2830 | 3628 | 22 | 3828 | 4913 | 22 |
| 80 | 1394 | 1567 | 11 | 2078 | 2726 | 24 | 2898 | 3891 | 26 | 3915 | 5213 | 25 |

**Table 12:** Comparison of the new table for $^{137}Cs$ and P-P table [1]

| Area ($cm^2$) | Distance from the planar implant (cm) | | | | | | | | | | | |
|---|---|---|---|---|---|---|---|---|---|---|---|---|
| | 1 | | | 2 | | | 3 | | | 4 | | |
| | Updated | P-P | Diff% | Updated | P-P | Diff% | Updated | P-P | Diff% | Updated | P-P | Diff% |
| 2 | 258 | 227 | -14 | 657 | 632 | -4 | 1311 | 1274 | -3 | 2238 | 2172 | -3 |
| 3 | 284 | 263 | -8 | 692 | 689 | 0 | 1350 | 1331 | -1 | 2279 | 2241 | -2 |
| 4 | 310 | 296 | -5 | 726 | 743 | 2 | 1389 | 1388 | 0 | 2320 | 2307 | -1 |
| 5 | 315 | 326 | 3 | 731 | 787 | 7 | 1394 | 1436 | 3 | 2326 | 2369 | 2 |
| 6 | 319 | 354 | 10 | 736 | 832 | 12 | 1400 | 1495 | 6 | 2331 | 2432 | 4 |
| 7 | 324 | 382 | 15 | 741 | 870 | 15 | 1405 | 1547 | 9 | 2337 | 2490 | 6 |
| 8 | 328 | 409 | 20 | 746 | 910 | 18 | 1410 | 1596 | 12 | 2342 | 2548 | 8 |
| 9 | 333 | 434 | 23 | 751 | 946 | 21 | 1415 | 1645 | 14 | 2348 | 2605 | 10 |
| 10 | 337 | 461 | 27 | 756 | 982 | 23 | 1421 | 1692 | 16 | 2353 | 2660 | 12 |
| 20 | 448 | 682 | 34 | 914 | 1303 | 30 | 1614 | 2106 | 23 | 2571 | 3155 | 19 |
| 30 | 571 | 846 | 33 | 1088 | 1582 | 31 | 1825 | 2468 | 26 | 2810 | 3562 | 21 |
| 40 | 694 | 994 | 30 | 1209 | 1843 | 34 | 2018 | 2787 | 28 | 3025 | 3931 | 23 |
| 50 | 817 | 1141 | 28 | 1383 | 2083 | 34 | 2180 | 3082 | 29 | 3198 | 4275 | 25 |
| 60 | 939 | 1283 | 27 | 1553 | 2319 | 33 | 2355 | 3362 | 30 | 3391 | 4605 | 26 |
| 70 | 1088 | 1426 | 24 | 1745 | 2532 | 31 | 2581 | 3628 | 29 | 3645 | 4913 | 26 |
| 80 | 1256 | 1567 | 20 | 1956 | 2726 | 28 | 2827 | 3891 | 27 | 3920 | 5213 | 25 |

of these calculations were compared with the values obtained using the recommended distribution by Paterson and Parker (Table 1).

Comparison of dose profiles indicated that selection of a suitable distribution of source strengths in a planar implant depends not only on the distance from the implant but also on type of the radionuclide source. Figure 4 shows that for a 7×7 $^{192}$Ir implant (42 cm$^2$) a 2/3×1/3 source strength distribution would provide a larger coverage area than a 1/2×1/2 scheme recommended by Paterson-Parker, at both 0.5 cm and 1.0 cm away from the plane of the implant. In addition, Figure 5 shows that for a 56 cm$^2$ planar implant with $^{137}$Cs source, a 2/3×1/3 source strength distribution scheme would provide a smaller dose coverage area than an $^{192}$Ir implant with the same area. These variations could be partially attributed to the differences in radial dose function of the two sources used, *i.e.*, $g_L$(r=6 cm) is 0.946 and 0.991 for $^{137}$Cs and $^{192}$Ir, respectively.

Table 2 shows an excellent agreement (within 2%) of the dose rate constants for $^{137}$Cs and $^{192}$Ir sources with the data published by Perez, *et al* [7], and Granero, *et al* [9], respectively. Moreover, Figure 6 shows the agreement of Monte Carlo simulated radial dose function of $^{137}$Cs and $^{192}$Ir sources obtained in this study and the data published by Perez, *et al* [7], and Granero, *et al* [9], respectively. Similarly, Figure 7 shows the agreement of Monte Carlo simulated 2D anisotropy functions with the published data. With completion of this validation process, the simulated dose profile of a 5×5 source $^{192}$Ir implant (20 cm$^2$) and 4×8 source $^{137}$Cs implant (56 cm$^2$) were compared with the calculated data using the TG-43U1 parameters using a 2/3×1/3 source strength distribution (Tables 3 4). The results reflected a good agreement between the two sets of data (within ±3%). Tables 5 and 6 shows the agreement (within ±2%) of the data obtained from the treatment planning software and the TG-43U1 parameter based dose profile for a 10×10 (90 cm$^2$) and 5×5 (20 cm$^2$) $^{192}$Ir implant, respectively. Similar agreement was observed for $^{137}$Cs source (Table 7).

After confirming the accuracy of the dose calculation methodology, the updated Paterson- Parker table was generated (Tables 8 and 9) using the optimal distribution of the source strengths that was extracted (Table 9) from the comparison of the dose profiles for each implant area. Tables 11 and 12 show the differences between the updated Paterson-Parker table and the original data for $^{192}$Ir and $^{137}$Cs sources, respectively. These observed differences may be attributed to the differences between the source dosimetric information and also to the selection of distribution of source strength that provide a better coverage of doses for each isotope. Figure 8 shows a comparison of the mg-hrs of $^{137}$Cs and $^{192}$Ir sources needed for delivering 1000 cGy at 1 cm away from a planar implant. These results indicated that the total mg-hr needed for an implant with $^{137}$Cs is not identical to that with $^{192}$Ir, due to the doimetric differences between the two sources.

In summary, an updated Paterson-Parker table was generated using the most recent published TG-43U1 dosimetric parameters of $^{137}$Cs and $^{192}$Ir sources. In addition to the central axis, dose profiles in two orthogonal directions were utilized to extract a better coverage of the treatment area. The results indicated that the mg-hrs used for $^{137}$Cs source in a planar implant is lesser than that of the mg-hrs needed for $^{192}$Ir to achieve the same dose coverage.

## Acknowledgements

The authors would like to thank Mr. Muhammad Ali Shah, Shahid B. Awan and David Soleimani-Meigooni for their valuable comments and suggestions during the preparation of this manuscript. In addition, the authors would like to appreciate the support and assistance of Miss Samira Sina, Miss Anahita Hajizadeh, Mr. Mehdi Zehtabian and Mr. Milad Baradarn.

## References


1. Paterson JR, Parker HM. A dosage for gamma-ray therapy. *Br J Radiology* 1943;**7**:592–612.
2. Parker HM. A dosage system for interstitial Radium therapy. *Br J Radiology* 1983;**11**:252-66
3. Paterson JR. The treatment of malignant disease by Radium x-rays being a practice of radiotherapy. Londan, Edward Arnold **1948**.
4. Meredit WJ. Radium dosage the Manchester system. Edinburgh, Livingston, Inc. **1967**.
5. Nath R, Anderson LL, Luxton G, *et al*. Dosimetry of interstitial brachytherapy sources: Recommendation of the AAPM Radiation Therapy Committee Task Group No. 43. *Med Phys* 1995;**22**:209-33.
6. Rivard MJ, Coursey BM, DeWerd LA, *et al*. Update of AAPM Task Group No. 43 Report: A revised AAPM protocol for brachytherapy dose calculations. *Med Phys* 2004;**31**:663-74.
7. Pérez-Calatayud J, Granero D, Ballester F, *et al*. Technical note: Monte Carlo derivation of TG-43 dosimetric parameters for radiation therapy resources and 3M Cs-137 sources. *Med Phys* 2005;**32**:2462-70.
8. Meigooni AS, Wright C, Koona RA, *et al*. TG-43U1 Based Dosimetric Characterization of Model 67-6520 Cs-137 Brachytherapy Source. *Med Phys* 2009;**36**:4711-19.
9. Granero D, Pérez-Calatayud J, Casal E, *et al*. A dosimetric study on the Ir-192 high dose rate Flexisource. *Med Phys* 2006;**33**:4578-82.
10. Liu L, Prasad SC, Bassano DA. Determination of 137Cs dosimetry parameters according to the AAPM TG-43 formalism. *Med Phys* 2004;**31**: 477-83.
11. Medich DC, Munro JJ. Monte Carlo characterization of the M-19 high dose rate Iridium-192brachytherapy source. *Med Phys* 2007;**34**:1999-2006.
12. National Nuclear Data Centre [Internet]. New York: Nuclear data from NuDat; Brookhaven National Laboratory. Available from: *www.nndc.bnl.gov/nudat2*.
13. Baltas D, Karaiskos P, Papagiannis P, *et al*. Beta versus gamma Dosimetry close to Ir-192 brachytherapy sources. Med Phys 2001;**28**:1875-82.
14. Hubble JH, Seltzer SM. National Institute of Standards and Technology[Internet]. [Place unknown]:Tables of x-ray mass attenuation coefficients and mass energy-absorption coefficients 1 keV to 20 MeV for elements Z=1 to 92 and 48 additional substances of dosimetric interest; 1996. Available from: *www.nist.gov/pml/data/xraycoef/index.cfm*
15. Zhang H, Baker C, McKinsy R, Meigooni AS. Dose verification with Monte Carlo technique for prostate brachytherapy implants with $^{125}$I sources. Medical Dosimetry 2005;**30**:85-91.
16. Quimby EH. Dosage calculations in Radium therapy. "Physical Foundations of Radiology **1952**;339-72.
17. Pierquin B, Dutreix A, Paine C. The paris system in interstitial radiation therapy. *Acta Radiol Oncol Biol. Radiat Phys* 1978;**17**:33-48.
18. Williamson JF, Morin RL, Khan FM. Monte Carlo evaluation of the Sievert integral for brachytherapy dosimetry. *Phys Med Biol* 1983;**28**:1021-3.
19. Butson MJ, Yu PKN, Cheung T, Metcalfe P. Radiochromic film for medical radiation dosimetry. *Mater Sci Eng R* 2003;**41**:61–120.
20. Devic S, Seuntjens J, Sham E, *et al*. Precise radiochromic film dosimetry using a flat-bed document scanner. *Med Phys* 2005;**32**: 2245-53.
21. Stevens MA, Turner JR, Hugtenburg RP, Butler PH. High-resolution dosimetry using radiochromic film and a document scanner. *Phys Med Biol* 1996;**41**;2357-65.
22. Gillin MT, Kline RW, Wilson JF, Cox JD. "Single and double plane implants: a comparison of the Manchester System with the Paris System," *Int J Radiat Oncol Biol Phys* 1984;**10**;921-5.